Schizophrenia Bulletin Advance Access published December 28, 2014
Schizophrenia Bulletin
doi:10.1093/schbul/sbu177

Patterns of Gray Matter Abnormalities in Schizophrenia Based on an International Mega-analysis

Cota Navin Gupta[1], Vince D. Calhoun[1–5], Srinivas Rachakonda[1], Jiayu Chen[1], Veena Patel[1], Jingyu Liu[1,3], Judith Segall[1], Barbara Franke[6,7], Marcel P. Zwiers[7], Alejandro Arias-Vasquez[6], Jan Buitelaar[7], Simon E. Fisher[7,8], Guillen Fernandez[7], Theo G. M. van Erp[9], Steven Potkin[9], Judith Ford[10], Daniel Mathalon[10], Sarah McEwen[11], Hyo Jong Lee[12], Bryon A. Mueller[13], Douglas N. Greve[14], Ole Andreassen[15,16], Ingrid Agartz[15,17,18], Randy L. Gollub[14,19], Scott R. Sponheim[13,20], Stefan Ehrlich[14,21], Lei Wang[22,23], Godfrey Pearlson[5,24,25], David C. Glahn[5,24], Emma Sprooten[5,24], Andrew R. Mayer[1], Julia Stephen[1], Rex E. Jung[26], Jose Canive[2,4,27], Juan Bustillo[2,4], and Jessica A. Turner*[,1,28]

[1]The Mind Research Network, Albuquerque, NM; [2]University of New Mexico Health Sciences Center, Albuquerque, NM; [3]Department of Electrical and Computer Engineering, University of New Mexico, Albuquerque, NM; [4]Department of Psychiatry, University of New Mexico, Albuquerque, NM; [5]Department of Psychiatry, School of Medicine, Yale University, New Haven, CT; [6]Department of Psychiatry and Human Genetics, Radboud University Nijmegen Medical Centre, Nijmegen, The Netherlands; [7]Department of Cognitive Neuroscience, Donders Institute for Brain, Cognition and Behavior, Radboud University Nijmegen Medical Center, Nijmegen, The Netherlands; [8]Department of Language and Genetics, Max Planck Institute for Psycholinguistics, Nijmegen, The Netherlands; [9]Department of Psychiatry & Human Behavior, School of Medicine, University of California, Irvine, CA; [10]Department of Psychiatry, School of Medicine, University of California, San Francisco, CA; [11]Department of Psychiatry & Biobehavioral Sciences, University of California, Los Angeles, CA; [12]Division of Electronics and Information Engineering, Chonbuk National University, Jeonju, Korea; [13]Department of Psychiatry, University of Minnesota, Minneapolis, MN; [14]MGH/MIT/HMS Athinoula A. Martinos Center for Biomedical Imaging, Charlestown, MA; [15]NORMENT, KG Jebsen Center for Psychosis Research, Institute of Clinical Medicine, University of Oslo, Oslo, Norway; [16]Division of Mental Health and Addiction, Oslo University Hospital, Oslo, Norway; [17]Department of Clinical Neuroscience, Karolinska Institutet, Stockholm, Sweden; [18]Department of Research, Diakonhjemmet Hospital, Oslo, Norway; [19]Department of Psychiatry, Massachusetts General Hospital, HMS, Boston, MA; [20]Minneapolis VA Healthcare System, Minneapolis, MN; [21]Department of Child and Adolescent Psychiatry, University Hospital Carl Gustav Carus, Dresden University of Technology, Dresden, Germany; [22]Department of Psychiatry and Behavioral Sciences, Northwestern University, Chicago, IL; [23]Department of Radiology, Northwestern University, Chicago, IL; [24]Institute of Living, Hartford Healthcare Corporation, Hartford, CT; [25]Department of Neurobiology, School of Medicine, Yale University, New Haven, CT; [26]Department of Neurosurgery, University of New Mexico Health Sciences Center, Albuquerque, NM; [27]Raymond G. Murphy VA Medical Center, Albuquerque, NM; [28]Department of Psychology and Neuroscience Institute, Georgia State University, Atlanta, GA

*To whom correspondence should be addressed; Department of Psychology, Georgia State University, PO Box 5010, Atlanta, GA 30302-5010, US; tel: 404-413-6211, fax: 404-413-6207, e-mail: jturner@mrn.org

Analyses of gray matter concentration (GMC) deficits in patients with schizophrenia (Sz) have identified robust changes throughout the cortex. We assessed the relationships between diagnosis, overall symptom severity, and patterns of gray matter in the largest aggregated structural imaging dataset to date. We performed both source-based morphometry (SBM) and voxel-based morphometry (VBM) analyses on GMC images from 784 Sz and 936 controls (Ct) across 23 scanning sites in Europe and the United States. After correcting for age, gender, site, and diagnosis by site interactions, SBM analyses showed 9 patterns of diagnostic differences. They comprised separate cortical, subcortical, and cerebellar regions. Seven patterns showed greater GMC in Ct than Sz, while 2 (brainstem and cerebellum) showed greater GMC for Sz. The greatest GMC deficit was in a single pattern comprising regions in the superior temporal gyrus, inferior frontal gyrus, and medial frontal cortex, which replicated over analyses of data subsets. VBM analyses identified overall cortical GMC loss and one small cluster of increased GMC in Sz, which overlapped with the SBM brainstem component. We found no significant association between the component loadings and symptom severity in either analysis. This mega-analysis confirms that the commonly found GMC loss in Sz in the anterior temporal lobe, insula, and medial frontal lobe form a single, consistent spatial pattern even in such a diverse dataset. The separation of GMC loss into robust, repeatable spatial patterns across multiple datasets paves the way for the application of these methods to identify subtle genetic and clinical cohort effects.

Key words: independent component analysis/schizophrenia/source-based morphometry/symptoms/voxel-based morphometry

Introduction

Numerous studies and meta-analyses of structural magnetic resonance imaging (MRI) in schizophrenia (Sz) report morphological brain differences,[1–9] including decreases in whole brain volume (~3%), gray matter concentration (GMC) (~2%), and white matter (~1%).[6] The largest cortical GMC deficits reported are in the left insular cortex, left inferior frontal gyrus, superior temporal gyrus, and precentral gyrus, according to a recent meta-analytical review.[7] Few studies have reported increased GMC in Sz; and the regions implicated were more discrete and smaller compared with decreased GMC regions. Sz may be associated with progressive cortical GMC loss,[9] though cross-sectional studies often cannot disentangle the effects of age and illness duration due to their high correlation.[10]

Voxel-based morphometry (VBM) is an automated technique which starts with a segmentation of the brain image into voxelwise measures of GMC or gray matter volume (GMV).[11] These measures can then be analyzed with univariate tests to identify clusters of voxels where Sz show gray matter changes relative to healthy subjects. Many large scale studies[3,12,13] and meta analyses[7] have established the effectiveness of VBM analyses for Sz research. While both measures are informative, GMC and GMV may actually track different pathological processes; GMC has previously led to more robust and spatially consistent findings than GMV and can be a more sensitive measure in Sz.[14,15] The univariate analyses on GMC measures show that many subcortical and cortical regions are affected in chronic Sz; however, they do not determine whether subsets of regions show similar patterns of deficits across individuals.

Clustering GMC deficits into spatial patterns can simplify the search for structural biomarkers, combining multiple regions into a single measure. Rather than considering a single region or subregion in isolation, identifying regions that show similar patterns of GMC loss is an efficient dimensional reduction in the space of potential biomarkers.[16] Source-based morphometry (SBM) is a multivariate extension of VBM utilizing spatially independent component analysis to obtain patterns of common GMC variation among participants.[17] This multivariate technique can improve sensitivity by parceling noise and scanner effects into separate components,[5] and by reducing the number of corrections for multiple statistical tests. Two previous SBM studies identified 5[17] and 4[5] spatial patterns that showed group differences in sample sizes of 240[17] and 635 participants,[5] respectively; these components comprised the bilateral temporal lobes, thalamus, basal ganglia, parietal lobes, and frontal/temporal regions. Determining that these multivariate methods can be used in large, aggregated datasets will be a practical step in exploring genetic influences, disease or medication effects, or possibly identifying areas that exhibit similar developmental trajectories.

The recent spurt in collaborative studies and the need to combine images from multiple sites (ie, an aggregated dataset) in order to increase statistical power[3,5,18,19] have encountered several challenges, due in part to inherent methodological differences in scanners and imaging parameters.[18,20,21] Most multisite imaging studies, particularly in Sz, have combined a relatively small number of sites (fewer than 10).[3,5,17] Large scale multisite integration has been successfully achieved for Alzheimer's and Huntington disorders in ADNI (30 sites)[22] and PREDICT-HD (32 sites),[23] respectively. However, these studies were prospective, requiring sites to collect data based on an agreed-upon protocol. We present the first Sz study that integrates legacy structural imaging data from across a broad selection of international sites in a single analysis.

A prominent issue in multisite Sz studies is the use of different scales for assessing psychotic symptoms. Three commonly used scales are the Scale for Assessment of Positive Symptoms (SAPS)/Scale for Assessment of Negative Symptoms (SANS), the Brief Psychiatric Rating Scale, and the Positive and Negative Syndrome Scale (PANSS).[24,25] Combining these scales is necessary for collaborative multisite research. Recent work[26] provides equations for converting symptoms ratings between scales, enabling us to perform a unified analysis in the present report.

The current article addresses some of the above issues by aggregating a very large dataset from 23 sites (1720 participants) and using SBM analysis in order to determine spatial patterns of GMC differences in Sz. We also performed a VBM analysis on the aggregated dataset to observe the overlap of spatial regions between both methodologies. This work also determines the relationship between regions showing group differences and symptom severity scores. We present the SBM technique as an effective framework for the integration of multisite data to obtain spatial patterns showing diagnostic group differences, thereby bringing this approach into the realm of the larger mega-analytic VBM studies.

Methods

Subject Demographics

Each legacy dataset including diagnosis, age at time of scan, gender, illness duration, symptom scores, and current medications when available, was shared by each research group according to their site's protocols. Thorough details regarding the samples have been published in the studies cited in the supplementary appendix 1. The majority of Sz were on antipsychotic medications, either typical, atypical, or a combination. All Sz were clinically stable at the time of scanning. A total of 936

structural MRI images of Ct (mean age = 34.81, SD = 11.89, range: 13–80) and 784 Sz (mean age = 36.65, SD = 11.62, range: 17–64) from 8 independent studies (several being multisite) formed the aggregated dataset, which totaled to 23 scanning sites. The study-wise demographics are given in table 1. All studies were collected under local institutional review board oversight and all participants provided informed consent.

All studies used the Structured Clinical Interview for Diagnosis for DSM-IV or DSM-IV-TR to confirm a diagnosis of Sz or schizoaffective disorder. Four studies rated symptoms using the PANSS, while the rest used SANS/SAPS scales as indicated in table 2. To enable mega-analysis, all SANS/SAPS scales were converted to PANSS positive and negative scores, using the between-scale symptom rating conversions implemented at http://www.converteasy.org.[26]

Imaging Methods

The scanning sites utilized 1.5T and 3T scanners of various makes and models, collecting T1-weighted images using a variety of scanning orientation and pulse sequences; see supplementary appendix 1 for details and previous publications. According to the methods presented in references[3,5,17], images were normalized using a 12-parameter affine model to the 152 average T1 Montreal Neurological Institute (MNI) template, resliced to 2 × 2 × 2 mm, and segmented into gray, white, and cerebral spinal fluid images using the unified segmentation algorithm[11] of SPM5 (http://www.fil.ion.ucl.ac.uk/spm/software/spm5/). We used the same standard preprocessing pipeline from our previous studies[3,5,27] which included several of the current datasets. While there may be distortion differences across scanners, we had observed that preprocessing (ie, usage of modulated or unmodulated data) does not have a strong effect on SBM spatial patterns in our previous study.[27] Outlier GMC images were identified based on correlations to both a study-specific template and an averaged GMC map[3] from all studies. Outliers were then visually checked, corrected, and resegmented where possible, and removed in cases where correction was not possible. The sample sizes presented in table 1 are those images which passed the quality assurance methods.

Age and gender affect GMC[5,17,28,29] and thereby SBM components. The effects of intersite differences also need to be considered; multisite structural studies have reported differences between sites, though not interactions between site and diagnosis, age, gender, or other variables.[3,30] Our initial analyses presented in Cota et al[31] indicated that linearly regressing age and gender from the images prior to SBM analysis can make the results more sensitive to group differences, while site effect estimates can be noisy for small datasets. Thus we regressed out age and gender of the images voxelwise prior to further analysis, while site and site by diagnosis terms were included in the VBM and SBM analyses models. A full width half maximum Gaussian kernel of 10 mm was used to smooth the images prior to the VBM and SBM analyses, as suggested in previous studies.[2,3,32]

SBM Analysis

In spatial independent component analysis,[17] each subject's data is decomposed into a linear combination of components or patterns and normalized loading coefficients (ie, the weighting of each component in each subject's data). The SBM module of the GIFT Toolbox (http://mialab.mrn.org/software/gift/) was used to perform the independent component analysis decompositions on the aggregated dataset. A prior study has conducted a comprehensive overview of this algorithm's strengths and limitations.[17] The number of components was set to 30 as in earlier work,[5,17] and we used ICASSO (20 runs) to determine the stability of the components.[5] The SBM decomposition was performed on the aggregated dataset consisting of 784 Sz and 936 Ct from 23 sites. Artifact components were identified visually and not included in subsequent analyses. To confirm the robustness of these findings, we also performed separate SBM decompositions on each study's dataset.

Table 1. Demographic Information by Study

			Patients With Schizophrenia (Sz)			Controls (Ct)		
Study Name	Sample Size	Sites	M/F	Mean Age ± SD	Age (Min to Max)	M/F	Mean Age ± SD	Age (Min to Max)
FBIRN 3	356	8	137/44	39.14 ± 11.62	18–62	123/52	37.99 ± 11.30	19–60
TOP	314	1	80/53	31.84 ± 08.97	18–62	98/83	34.09 ± 09.14	17–55
HUBIN	195	1	70/24	41.63 ± 07.63	25–56	69/32	41.91 ± 08.86	19–56
MCIC	233	4	83/26	34.86 ± 11.03	18–60	75/49	32.27 ± 10.88	18–58
NW	189	1	73/25	33.61 ± 12.84	17–61	52/39	32.28 ± 14.50	14–68
OLIN	176	1	32/15	38.34 ± 11.74	18–60	95/34	28.25 ± 13.17	13–80
COBRE	156	1	64/13	37.46 ± 13.44	18–64	55/24	36.15 ± 11.73	18–65
FBIRN 2	101	6	27/18	38.02 ± 10.08	20–58	35/21	37.35 ± 10.59	20–59

Table 2. Summary of the Clinical Measures

Study Name	Original Scale Available for Symptoms	Sz	% Reporting (PANSS Positive)	PANSS Positive Mean ± SD	% Reporting (PANSS Negative)	PANSS Negative Mean ± SD	% Reporting (Duration of Illness)	DOI Mean ± SD
FBIRN3	PANSS	181	98.90	15.55 ± 5.11	98.90	14.40 ± 5.50	98.90	17.67 ± 11.60
TOP	PANSS	133	90.98	14.91 ± 5.34	92.48	15.20 ± 6.85	97.74	6.68 ± 5.83
HUBIN	SAPS/SANS	94	59.57	14.50 ± 2.99	61.70	17.56 ± 6.85	100.00	17.23 ± 8.53
MCIC	SAPS/SANS	109	100.00	16.79 ± 4.12	100.00	16.58 ± 4.39	99.08	12.10 ± 10.64
NW	SAPS/SANS	98	64.29	15.52 ± 3.44	69.39	16.10 ± 4.52	71.43	13.70 ± 12.59
COBRE	PANSS	77	97.50	15.60 ± 4.86	97.50	14.76 ± 4.94	98.70	15.66 ± 11.82
FBIRN2	SAPS/SANS	48	89.51	16.17 ± 3.00	91.67	13.39 ± 3.46	N/A	N/A
OLIN	PANSS	47	42.55	16.6 ± 4.44	42.55	17.2 ± 6.46	N/A	N/A

Note: N/A, not available PANSS, Positive and Negative Syndrome Scale; SANS, Scale for Assessment of Negative Symptoms; SAPS, Scale for Assessment of Positive Symptoms; Sz, schizophrenia.

A larger loading coefficient for an individual or group indicates that the spatial pattern is more strongly weighted in the data for that individual or group. However, the interpretation of the loading coefficient difference depends upon the spatial image of the component. If the spatial component is predominantly positive, and if the loading coefficients are greater in Ct than in Sz, we infer that GMC is greater in Ct for the spatial component under consideration.

We examined the differences in loading coefficients from Sz and Ct participants using SPSS.[33] A multivariate analysis of covariance (MANCOVA) model was used with SBM coefficients as dependent variables, diagnosis as a factor, site as a dummy-scored covariate, and site by diagnosis as an interaction. A threshold of $P < .05$ corrected for multiple testing using the false discovery rate (FDR) method[34] was used to find components showing a significant effect of diagnosis. To confirm these findings further we also performed independent SBMs on each of the 8 studies, to determine if the same components showed group differences at an uncorrected $P < .05$.

Correlates of Clinical Variables With SBM Loadings

The clinical correlation analysis between the SBM components showing Ct/Sz difference and the PANSS positive and negative scores were set up as 2 models in SPSS.[33] A MANCOVA was used with the dependent variables being SBM component loadings, while the covariates were site and PANSS positive or negative scores. The model included the interaction term between site and clinical scores. FDR correction for multiple comparisons was used to find significant associations between the SBM components and clinical parameters.

VBM Analysis

We performed a univariate VBM analysis on the aggregated dataset as per previous protocols,[3,5] using the SPM5 software. The smoothed GMC images regressed for age and gender, from the sites having both cases and control data, were used in a general linear model. Diagnosis and dummy-coded scanning site were factors.[19,35] Statistical results for group comparisons were thresholded at an FDR-corrected $P < .05$ and an extent threshold of 5 voxels. For clinical analysis, we used a regression model in SPM5, with clinical score vs the smoothed GMC images regressed for age and gender, and site as the covariate.

Results

SBM Results and Correlates With Clinical Variables

The aggregated dataset from 8 studies in table 1 was decomposed into 30 SBM components. On visual inspection we identified 2 components suggestive of obvious artifacts, ie, having spatial patterns primarily around the

edges of the brain or in white matter regions,[17] which were removed. In the remaining components we observed 9 spatial patterns showing a significant effect of diagnosis. Figure 1 and table 3 depict the 9 spatial patterns and their brain regions (having volumes greater than 1 cm^3), ordered by decreasing effect sizes using partial eta squared.[33] All maps in figure 1 were thresholded at $|z| > 2.5$ (ie, the voxels shown are the ones that contribute strongly to these components). Seven of these components contained areas where GMC values were greater in Ct than Sz; 2 components had areas where GMC was higher in Sz than Ct. The brain labels in table 3 were obtained from the Talairach Daemon (http://www.talairach.org/daemon.html) based on the transformed locations of the

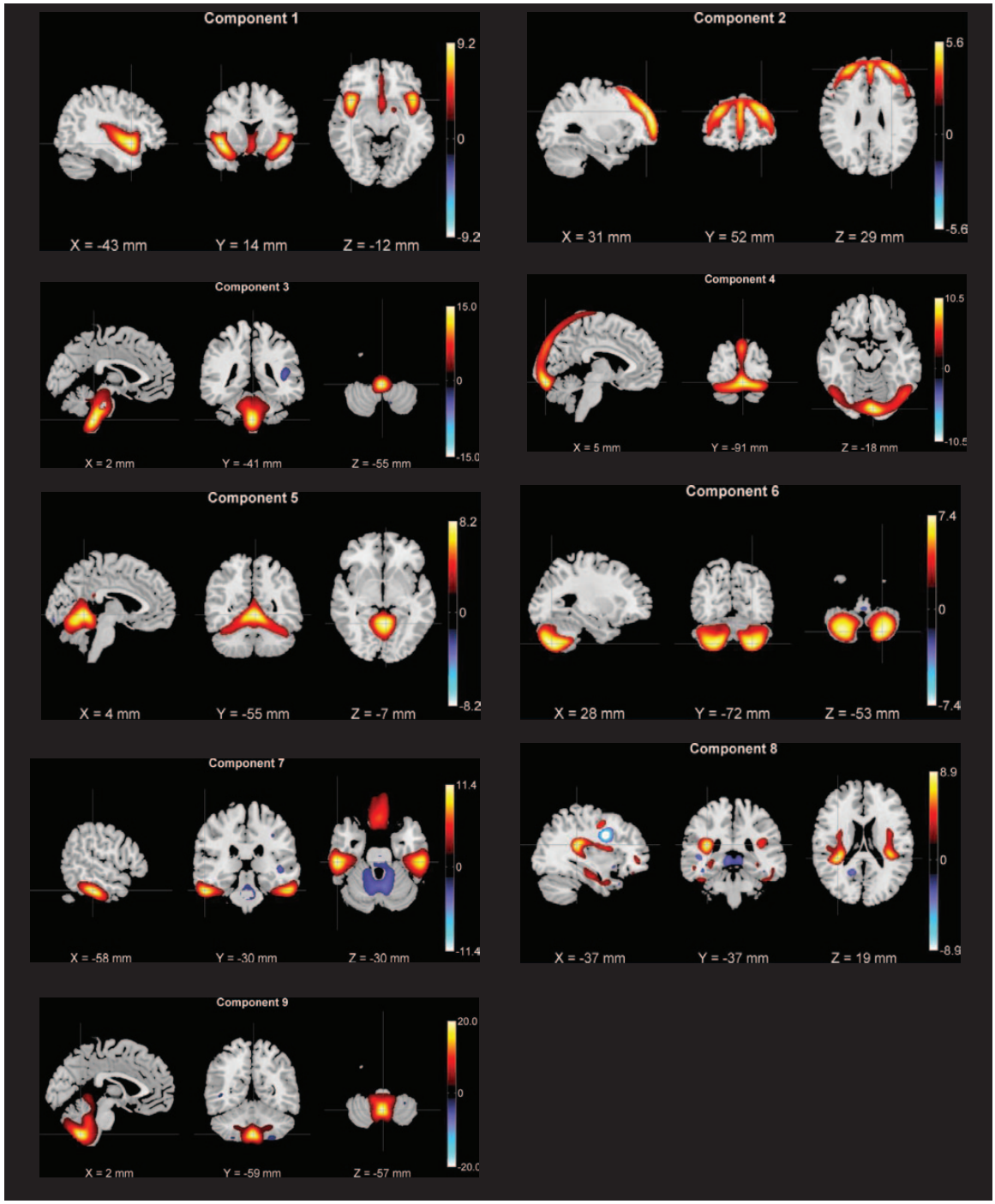

Fig. 1. Spatial maps of the 9 components showing (Ct/Sz) group effect, ordered by decreasing effect size from the primary SBM decomposition. All are thresholded at $|z| > 2.5$. The color bar indicates the color mapping for the normalized component weights. Ct, control; SBM, source-based morphometry; Sz, schizophrenia.

Table 3. Loading Directionality and Brain Labels for the ICA Components Showing Ct/Sz Difference (Numbered in the Order of Decreasing Effect Sizes)

Component Number	Effect Size (Partial Eta Squared)	Loadings Directionality	Brain Region Label (Positive/Negative)	L/R Volume (cm^3)	Brodmann Area	L/R: Max Z Value (x, y, z)
1	0.048	Ct > Sz	Superior temporal gyrus	10.4/9.2	13,22,38,41,42	9.3 (−42, 13, −11)/8.1 (46, 11, −7)
			Inferior frontal gyrus	5.4/4.7	13,45,47	9.1 (−40, 13, −14)/8.4 (42, 15, −13)
			Insula	5.8/5.4	13	8.6 (−44, 2, −5)/7.2 (46, 8, −4)
2	0.033	Ct > Sz	Superior frontal gyrus	16.6/20.4	6,8,9,10,11	5.1 (−28, 52, 23)/5.7 (30, 52, 23)
			Middle frontal gyrus	14.5/17.7	6,8,9,10,46	5.1 (−28, 53, 19)/5.6 (30, 53, 19)
			Medial frontal gyrus	4.1/5.2	6,8,9,10,11	4.4 (0, 48, 20)/4.3 (4, 60, 3)
3	0.027	Sz > Ct	Brainstem	3.3/2.2	—	7.1 (−8, −40, −25)/6.1 (0, −42, −30)
4	0.009	Ct > Sz	Fusiform gyrus	3.3/4.4	18,19,37,20,36	6.8 (−20, −88, −16)/8.4 (20, −88, −14)
			Cuneus	0.8/2.6	17,18,19	5.2 (0, −93, 3)/6.9 (4, −93, 3)
			Precuneus	0.3/1.0	7,19	3.9 (−2, −78, 41)/5.9 (6, −81, 41)
5	0.007	Ct > Sz	Vermis	13.6/16.1	—	7.9 (−2, −53, −2)/8.3 (2, −53, −2)
			Declive	11.5/11.9	—	6.7 (0, −65, −12)/6.7 (4, −65, −12)
6	0.007	Sz > Ct	Cerebellum	7.2/7.1	—	6.4 (−30, −60, −42)/6.9 (28, −60, −39)
			Inferior semilunar lobule	7.8/8.6	—	7.1 (−26, −70, −40)/7.4 (28, −72, −40)
7	0.006	Ct > Sz	Inferior temporal gyrus	2.9/3.1	20,37	11.2 (−57, −32, −22)/8.2(57, −28, −20)
			Fusiform gyrus	2.1/1.9	20,36,37	9.9 (−51, −25, −26)/10.1 (57, −32, −22)
8	0.004	Ct > Sz	Posterior insula	4.7/4.8	13,47	9.1 (−36, −34, 18)/8.0 (36, −28, 20)
			Superior temporal gyrus	1.7/0.6	41,13,21,22,38	8.4 (−38, −36, 15)/5.3 (36, −32, 16)
			Middle frontal gyrus	2.4/2.3	6,8,10,11	7.6 (−30, 2, 44)/6.1 (28, 6, 44)
			Hippocampus	3.3/2.5	19,28,30,34,35,36,37	4.7 (−34, −17, −21)/4.2 (34, −15, −23)
			Precentral gyrus	***1.5/0.8***	***6,9***	13.2 (−34, 5, 29)/9.6 (36, 3, 29)
			Inferior frontal gyrus	***2.0/1.2***	***9,47***	11.3 (−38, 5, 29)/11.2 (36, 7, 29)
9	0.004	Ct > Sz	Inferior semilunar lobule	1.0/1.8	—	15.3 (−4, −58, −42)/15.6 (4, −58, −42)
			Cerebellar tonsil	2.2/2.2		11.5 (0, −50, −38)/10.0 (4, −51, −40)

Note: Negative component regions in bold italic. Ct, control; ICA, independent component analysis; Sz, schizophrenia.

largest clusters in the component maps and were visually confirmed using Mricron (http://www.mccauslandcenter.sc.edu/mricro/mricron/).

The replication of patterns from independent SBM decompositions across studies depicted in supplementary appendix 2 showed that components 1, 2, 3, and 9 were consistent. In particular, the top 3 components replicated across at least 5 of the 8 studies, passing an uncorrected $P < .05$. Given the combination of sites, field strengths, and sequence differences, we also performed secondary analyses of the loading coefficients modeling 1.5T vs 3T scanners, or within the 1.5T sites including scanning sequence as a factor rather than including site per set. The same components were still significant in those models and there were not scanner × diagnosis interactions which changed the order of the effects. Those results are included in supplementary appendix 2.

We discuss the components ordered by their effect sizes. The largest GMC difference between diagnostic groups was found in component 1, comprising regions in the superior temporal gyrus, inferior frontal gyrus, and insula. Ct had greater loading coefficients than Sz for this component ($F(1,1716) = 86.27$, $P < .0001$, partial eta squared = 0.048), implying that these areas formed a consistent spatial grouping and showed a greater GMC in Ct than Sz.

Component 2 was localized primarily in regions of superior frontal gyrus, middle frontal gyrus, and medial frontal gyrus ($F(1,1716) = 55.93$, $P < .0001$, partial eta squared = 0.032) with a loading directionality of Ct > Sz.

Component 3 covered regions of the brainstem ($F(1,1716) = 47.78$, $P < .0001$, partial eta squared = 0.027) wherein Sz participants showed larger loading coefficients than did Ct, implying that the component regions showed more GMC in Sz than Ct.

Component 4 covered the cuneus, precuneus, and fusiform gyrus ($F(1,1716) = 15.55$, $P < .0001$, partial eta squared = 0.009), while component 5 covered the regions of vermis and declive ($F(1,1716) = 11.69$, $P = .001$, partial eta squared = 0.007). For both these components the loading directionality observed was Ct greater than Sz.

Component 6 covered the regions of cerebellum and inferior semilunar lobule ($F(1,1716) = 12.64$, $P < .0001$, partial eta squared = 0.007). The directionality of loading coefficients was Sz greater than Ct, indicating patients with Sz had more GMC in these regions than Ct. This was the only component which had a significant site by diagnosis interaction effect ($F(1,1716) = 8.27$, $P = .004$, partial eta squared = 0.005).

Component 7 covered the regions of inferior temporal gyrus and fusiform gyrus ($F(1,1716) = 10.727$, $P = .001$, partial eta squared = 0.006). The loading directionality for this component was Ct greater than Sz.

Component 8 had both positive and negative voxels ($F(1,1716) = 6.09$, $P = .014$, partial eta squared = 0.004). The positive regions included posterior insula, superior temporal gyrus, hippocampus, and middle frontal gyrus, while the negative regions included precentral gyrus and inferior frontal gyrus. Component 9 covered the regions of inferior semilunar lobule and cerebellar tonsil ($F(1,1716) = 7.17$, $P = .007$, partial eta squared = 0.004). Both these components had a loading directionality of Ct greater than Sz.

The SPSS analysis of these 9 component loadings with the PANSS positive and negative scores did not show any association that passed the corrected significance threshold. The corresponding scatter plots are included in supplementary appendix 3.

VBM Results

Figure 2a depicts regions showing differences in GMC for the Ct > Sz contrast ($P < .05$, FDR corrected; $k = 5$), that covered most of the brain in a single cluster. The maximal difference voxel was located at (39, 15, −5) mm in MNI space in between the right insula and putamen. The cluster wise P value was $P < 1 \times 10^{-7}$ (FDR corrected), with $t(1669) = 11.98$.

Figure 2b depicts the areas where Sz participants had greater values than Ct, which include the cerebellum and brainstem. The maximum voxel was located at (16, −42, −36) mm in MNI space. The cluster wise P value was $P < 1 \times 10^{-7}$ (FDR corrected) and $t(1669) = 8.40$, with 1608 voxels in the cluster. The overlap of regions from VBM analyses (contrast Sz > Ct) and the 2 SBM components having directionality Sz > Ct are shown in supplementary appendix 5.

Site by diagnosis effects were limited to 2 small clusters depicted in supplementary appendix 4. The first cluster was observed around the brainstem with 187 voxels having $F(20,1669) = 3.68$, and the maximum voxel located at (10, −20, −18) mm in MNI space. The second cluster with 183 voxels was observed around thalamus with the maximum voxel located at (−4, −14, 4) mm and having $F(20,1669) = 3.37$. The VBM analysis of positive or negative PANSS scores with GMC showed no significant results.

Discussion

This work is the largest Sz multisite structural imaging study to date, totaling 1720 participants (936 Ct/784 Sz) from 23 sites. We addressed the effects of imaging heterogeneity due to multisite acquisition by using a uniform preprocessing pipeline for the GMC images, with careful quality assurance, and by including site and site by diagnosis terms in the model. The SBM analysis grouped the GMC changes into 9 independent spatial components, while VBM analyses identified 1 massive cluster of GMC loss across the entire cortex. These components are areas of interrelated GMC differences, potentially identifying regions affected similarly by pathology, development, or

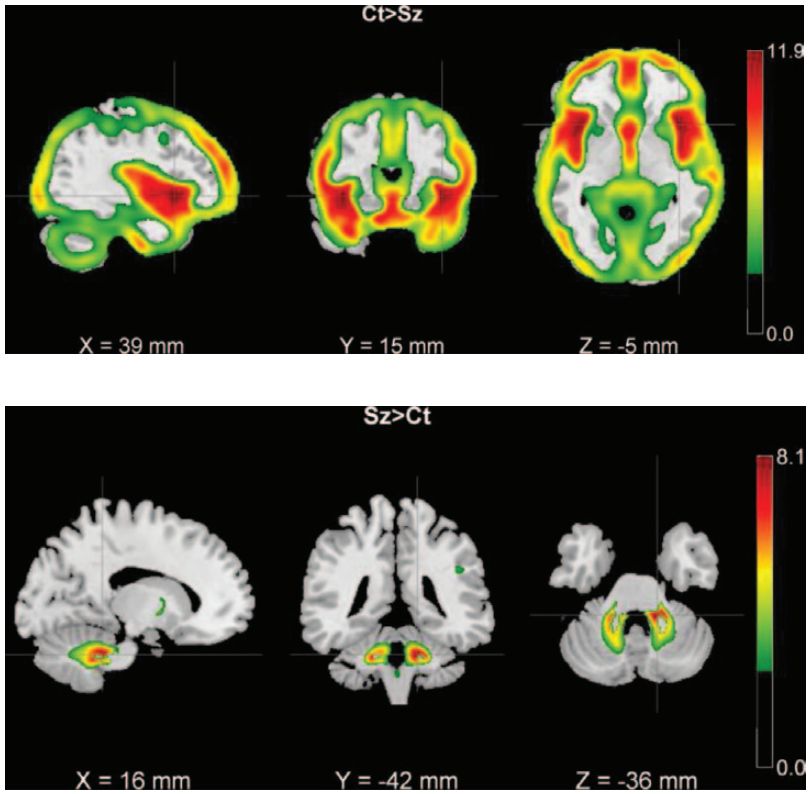

Fig. 2. Results of the VBM analysis; voxels above $|Z| > 2.5$ are shown. (a) Significant clusters where Ct > Sz. (b) Significant clusters where Sz > Ct. Ct, control; Sz, schizophrenia; VBM, voxel-based morphometry.

environmental effects. Seven of the identified SBM components showed less GMC in Sz, while 2 components (brainstem and cerebellum regions) had increased GMC in Sz. VBM identified the brainstem component showing greater GMC in Sz, but not the cerebellum regions which were delineated by SBM. No spatial patterns of GMC difference were related to the measures of symptom severity.

We found the largest GMC difference between diagnostic groups in the network including the superior temporal gyrus, inferior frontal gyrus, and insula (ie, component 1 in figure 1). This primary pattern unifies the findings in several previous VBM meta-analysis studies[2,6,7,9] into a single network. The regions identified by the VBM meta-analysis of Glahn et al[7] as decreased in Sz are also identified in this analysis, but in the SBM analysis they are grouped into networks combining the insula with superior temporal regions and inferior frontal gyrus, while the cerebellum, vermis, and inferior temporal gyrus are grouped into separate networks. This primary pattern of inferior frontal/insular regions, medial frontal, and superior temporal GMC loss has also been identified in our previous smaller SBM studies with partially overlapping data.[5,17] In one study[5] we also investigated the familiality of SBM components in sibling pairs, and an estimated 43% of the variance in the loadings for this component was attributable to the sibling relationships. Given the reproducibility and familiality of this component, we foresee enough motivation for this to be used as a potential endophenotype in future imaging genetics studies.

Our analysis showed 2 spatial patterns where Sz had greater GMC than Ct. The first, component 3 in figure 1, primarily covered the pons, extending into the ventral tegmental area. This is a region which can be noisy and subject to artifact, including possible breathing and heart rate differences, insofar as those affect a structural image. Alternatively, this area of increased GMC does overlap with the ventral tegmental nuclei responsible for dopamine production. These nuclei could be enlarged due to the illness, as increased release of dopamine in the striatum has been demonstrated in Sz independent of antipsychotic treatment.[36] Chronic exposure to dopamine D2-blocking therapeutic agents, the norm in our sample, may have resulted in miniscule compensatory increases in GMC around some brainstem regions. VBM results (for contrast Sz > Ct) also showed this region, with the overlap from both analyses depicted in supplementary appendix 5. Component 6 in figure 1, which covered the cerebellar regions, also showed greater GMC regions in Sz as observed in previous VBM studies.[37,38] However this region was not observed in our VBM analysis and did not show a trend toward significance in replication across studies (supplementary appendix 2), and thus should be interpreted with caution. We also observed abnormalities

of the cerebellar vermis in component 5, with Sz showing less GMC as previously reported.[39,40] With recent studies pointing to neuroanatomical evidence of closed-loop connectivity between prefrontal cortex and the cerebellar regions,[41–43] the understanding of these distributed network interactions may be critical to understanding Sz.

The observed 4th component extended up the posterior midline of the brain and was possibly artifactual. To confirm that this component captured the actual variation in the brain shape and had not merely identified participants who were poorly segmented, we examined images corresponding to the largest and smallest coefficients (3 in each case are depicted in supplementary appendix 6). In participants with the largest loadings, the posterior lobes had more GMC (their hemispheres filled the back of the brain more tightly), whereas the participants corresponding to the smallest loadings had larger gaps in the posterior midline. Thus, it appears this component captured true regional differences in posterior GMC.

While the analysis of positive and negative symptom severity did not show any relationship to either univariate or multivariate GMC loss in this sample, this may be due to differences in the implementation of these measures across sites and datasets. As an aggregation of legacy datasets, the data were collected at different times and without cross-study standardization in symptom assessment, which may have increased variation. However, the constructs of positive and negative symptoms are fairly broad and diffuse, capturing variable treatment response patterns. It is possible that since most of the Sz were many years into the disease, these questionnaires yield no additional information on brain structure variation. However, the relationship between these volumetric patterns and individual variation in more granular symptom measures (eg, disorganized thoughts vs hallucination severity), or individual cognitive deficits still needs to be explored in datasets for which those measures are available.

As is a common caveat in this work, all the Sz were on antipsychotic medications, and in certain datasets the amounts and history of dosage were not recorded. Further exploration of the interaction between medication dosage and duration of illness, in datasets where those measures are available, is needed for more nuanced analyses of these multivariate patterns of GMC loss. This kind of multisite mega-analysis highlights the need for standardized phenotyping. Availability of standardized chlorpromazine equivalents as well as common cognitive and clinical batteries would make the analysis easier and much more informative.

In summary, SBM is an effective technique delineating distinct and consistent anatomical brain regions that show difference between healthy Ct and patients with Sz. We have identified that the cortical, brainstem, and cerebellar areas of gray matter loss form highly replicable patterns across studies, and are not related to global measures of symptom severity. The regions of gray matter loss formed networks of anterior temporal, insular, and medial prefrontal regions, as well as parts of the frontal cortex, posterior brain regions, and several separate brainstem and cerebellar networks. These patterns of spatial components could serve as endophenotypes for Sz, indicating regions which are affected similarly by common causes such as genetics, disease progression, or medication. Future work may involve investigating differences between Sz subgroups as well as comparing patient subgroups with typical and atypical medication use, and finding associations between these imaging endophenotypes and genetic variability. Funding and citations for each dataset used in these analyses are provided in the supplementary material.

Supplementary Material

Supplementary material is available at http://schizophreniabulletin.oxfordjournals.org.

Funding

Primary funding for this project was provided by National Institute of Mental Health (1R01MH094524-01A1 to V.D.C. and J.A.T.).

Acknowledgment

The authors have declared that there are no conflicts of interest in relation to the subject of this study.

References

1. McCarley RW, Wible CG, Frumin M, et al. MRI anatomy of schizophrenia. *Biol Psychiatry*. 1999;45:1099–1119.
2. Honea R, Crow TJ, Passingham D, Mackay CE. Regional deficits in brain volume in schizophrenia: a meta-analysis of voxel-based morphometry studies. *Am J Psychiatry*. 2005;162:2233–2245.
3. Segall JM, Turner JA, van Erp TG, et al. Voxel-based morphometric multisite collaborative study on schizophrenia. *Schizophr Bull*. 2009;35:82–95.
4. Shenton ME, Dickey CC, Frumin M, McCarley RW. A review of MRI findings in schizophrenia. *Schizophr Res*. 2001;49:1–52.
5. Turner JA, Calhoun VD, Michael A, et al. Heritability of multivariate gray matter measures in schizophrenia. *Twin Res Hum Genet*. 2012;15:324.
6. Wright IC, Rabe-Hesketh S, Woodruff PW, David AS, Murray RM, Bullmore ET. Meta-analysis of regional brain volumes in schizophrenia. *Am J Psychiatry*. 2000;157:16–25.
7. Glahn DC, Laird AR, Ellison-Wright I, et al. Meta-analysis of gray matter anomalies in schizophrenia: application of anatomic likelihood estimation and network analysis. *Biol Psychiatry*. 2008;64:774–781.
8. Ellison-Wright I, Bullmore E. Anatomy of bipolar disorder and schizophrenia: a meta-analysis. *Schizophr Res*. 2010;117:1–12.
9. Vita A, De Peri L, Deste G, Sacchetti E. Progressive loss of cortical gray matter in schizophrenia: a meta-analysis

and meta-regression of longitudinal MRI studies. *Transl Psychiatry*. 2013;3:e275.
10. Premkumar P, Fannon D, Kuipers E, Cooke MA, Simmons A, Kumari V. Association between a longer duration of illness, age and lower frontal lobe grey matter volume in schizophrenia. *Behav Brain Res*. 2008;193:132–139.
11. Ashburner J, Friston KJ. Voxel-based morphometry–the methods. *Neuroimage*. 2000;11:805–821.
12. Hulshoff Pol HE, Schnack HG, Mandl RC, et al. Focal gray matter density changes in schizophrenia. *Arch Gen Psychiatry*. 2001;58:1118–1125.
13. Honea RA, Meyer-Lindenberg A, Hobbs KB, et al. Is gray matter volume an intermediate phenotype for schizophrenia? A voxel-based morphometry study of patients with schizophrenia and their healthy siblings. *Biol Psychiatry*. 2008;63:465–474.
14. Fornito A, Yücel M, Patti J, Wood SJ, Pantelis C. Mapping grey matter reductions in schizophrenia: an anatomical likelihood estimation analysis of voxel-based morphometry studies. *Schizophr Res*. 2009;108:104–113.
15. Meda SA, Giuliani NR, Calhoun VD, et al. A large scale (N=400) investigation of gray matter differences in schizophrenia using optimized voxel-based morphometry. *Schizophr Res*. 2008;101:95–105.
16. Nenadic I, Gaser C, Sauer H. Heterogeneity of brain structural variation and the structural imaging endophenotypes in schizophrenia. *Neuropsychobiology*. 2012;66:44–49.
17. Xu L, Groth KM, Pearlson G, Schretlen DJ, Calhoun VD. Source-based morphometry: the use of independent component analysis to identify gray matter differences with application to schizophrenia. *Hum Brain Mapp*. 2009;30:711–724.
18. Jovicich J, Czanner S, Greve D, et al. Reliability in multisite structural MRI studies: effects of gradient non-linearity correction on phantom and human data. *Neuroimage*. 2006;30:436–443.
19. de Wit SJ, Alonso P, Schweren L, et al. Multicenter voxel-based morphometry mega-analysis of structural brain scans in obsessive-compulsive disorder. *Am J Psychiatry*. 2014;171:340–349.
20. Stonnington CM, Tan G, Klöppel S, et al. Interpreting scan data acquired from multiple scanners: a study with Alzheimer's disease. *Neuroimage*. 2008;39:1180–1185.
21. Fennema-Notestine C, Gamst AC, Quinn BT, et al. Feasibility of multi-site clinical structural neuroimaging studies of aging using legacy data. *Neuroinformatics*. 2007;5:235–245.
22. Jack CR, Bernstein MA, Fox NC, et al. The Alzheimer's Disease Neuroimaging Initiative (ADNI): MRI methods. *J Magn Reson Imaging*. 2008;27:685–691.
23. Biglan KM, Zhang Y, Long JD, et al. Refining the diagnosis of Huntington disease: the PREDICT-HD study. *Front Aging Neurosci*. 2013;5:12.
24. Nesvåg R, Saetre P, Lawyer G, Jönsson EG, Agartz I. The relationship between symptom severity and regional cortical and grey matter volumes in schizophrenia. *Prog Neuropsychopharmacol Biol Psychiatry*. 2009;33:482–490.
25. Lyne JP, Kinsella A, O'Donoghue B. Can we combine symptom scales for collaborative research projects? *J Psychiatr Res*. 2012;46:233–238.
26. van Erp TG, Preda A, Nguyen D, et al. Converting positive and negative symptom scores between PANSS and SAPS/SANS. *Schizophr Res*. 2014;152:289–294.
27. Chen J, Liu J, Calhoun VD, et al. Exploration of scanning effects in multi-site structural MRI studies. *J Neurosci Methods*. 2014;230:37–50.
28. Segall JM, Allen EA, Jung RE, et al. Correspondence between structure and function in the human brain at rest. *Front Neuroinform*. 2012;6:10.
29. Haijma S, van Haren N, Cahn W, et al. Brain volumes in schizophrenia: a meta-analysis in over 18,000 subjects. *Schizophr Bull*. 2013;39:1129–1138.
30. Bockholt HJ, Turner JA, Johnson HJ, et al. Morphometric analysis of a multi-site study of schizophrenia using Freesurfer. Annual Meeting of the Society for Neuroscience, San Diego, CA, 2007.
31. Cota N, Rachakonda S, Calhoun VD, Turner JA. Application of source based morphometry for an aggregated/multisite gray matter dataset. *Schizophr Bull*. 2013;39(suppl 1):S180.
32. Salmond CH, Ashburner J, Vargha-Khadem F, Connelly A, Gadian DG, Friston KJ. Distributional assumptions in voxel-based morphometry. *Neuroimage*. 2002;17:1027–1030.
33. *IBM SPSS Statistics for Windows [computer program]. Version Version 22.0*. Armonk, NY: IBM Corp.
34. Genovese CR, Lazar NA, Nichols T. Thresholding of statistical maps in functional neuroimaging using the false discovery rate. *Neuroimage*. 2002;15:870–878.
35. Pell GS, Briellmann RS, Chan CH, Pardoe H, Abbott DF, Jackson GD. Selection of the control group for VBM analysis: influence of covariates, matching and sample size. *Neuroimage*. 2008;41:1324–1335.
36. Laruelle M, Abi-Dargham A, Gil R, Kegeles L, Innis R. Increased dopamine transmission in schizophrenia: relationship to illness phases. *Biol Psychiatry*. 1999;46:56–72.
37. Ha TH, Youn T, Ha KS, et al. Gray matter abnormalities in paranoid schizophrenia and their clinical correlations. *Psychiatry Res*. 2004;132:251–260.
38. Suzuki M, Nohara S, Hagino H, et al. Regional changes in brain gray and white matter in patients with schizophrenia demonstrated with voxel-based analysis of MRI. *Schizophr Res*. 2002;55:41–54.
39. Henze R, Brunner R, Thiemann U, et al. Gray matter alterations in first-admission adolescents with schizophrenia. *J Neuroimaging*. 2011;21:241–246.
40. Okugawa G, Nobuhara K, Takase K, Kinoshita T. Cerebellar posterior superior vermis and cognitive cluster scores in drug-naive patients with first-episode schizophrenia. *Neuropsychobiology*. 2007;56:216–219.
41. Watson TC, Becker N, Apps R, Jones MW. Back to front: cerebellar connections and interactions with the prefrontal cortex. *Front Syst Neurosci*. 2014;8:4.
42. Andreasen NC, Pierson R. The role of the cerebellum in schizophrenia. *Biol Psychiatry*. 2008;64:81–88.
43. Andreasen NC, O'Leary DS, Cizadlo T, et al. Schizophrenia and cognitive dysmetria: a positron-emission tomography study of dysfunctional prefrontal-thalamic-cerebellar circuitry. *Proc Natl Acad Sci USA*. 1996;93:9985–9990.